



## OPEN ACCESS

## EDITED BY

Weihu Ma,  
Ningbo No.6 Hospital, China

## REVIEWED BY

Zixing Meng,  
University of Chinese Academy of Sciences,  
China  
Qiang Luo,  
Zhoukou Central Hospital, China

## \*CORRESPONDENCE

Liangjie Lu  
✉ lhlluliangjie@nbu.edu.cn  
Kaifeng Gan  
✉ gankaifeng@163.com

<sup>†</sup>These authors have contributed equally to this work and share first authorship

RECEIVED 21 October 2025

REVISED 07 November 2025

ACCEPTED 13 November 2025

PUBLISHED 05 December 2025

## CITATION

Lian L, Xu D, He C, Luo Z, Yu H, Liu B, Zhou K, Lu L and Gan K (2025) Zinc oxide nanoparticle chelated phosphocreatine-grafted chitosan composite hydrogels for enhancing osteogenesis and angiogenesis in bone regeneration.  
*Front. Med.* 12:1729401.  
doi: 10.3389/fmed.2025.1729401

## COPYRIGHT

© 2025 Lian, Xu, He, Luo, Yu, Liu, Zhou, Lu and Gan. This is an open-access article distributed under the terms of the [Creative Commons Attribution License \(CC BY\)](https://creativecommons.org/licenses/by/4.0/). The use, distribution or reproduction in other forums is permitted, provided the original author(s) and the copyright owner(s) are credited and that the original publication in this journal is cited, in accordance with accepted academic practice. No use, distribution or reproduction is permitted which does not comply with these terms.

# Zinc oxide nanoparticle chelated phosphocreatine-grafted chitosan composite hydrogels for enhancing osteogenesis and angiogenesis in bone regeneration

Leidong Lian<sup>1†</sup>, Dingli Xu<sup>2†</sup>, Chaonan He<sup>3</sup>, Zhe Luo<sup>1,2</sup>, Han Yu<sup>2</sup>, Botao Liu<sup>2</sup>, Ke Zhou<sup>1</sup>, Liangjie Lu<sup>1\*</sup> and Kaifeng Gan<sup>1\*</sup>

<sup>1</sup>The Affiliated Lihuli Hospital of Ningbo University, Ningbo, Zhejiang, China, <sup>2</sup>Health Science Center, Ningbo University, Ningbo, China, <sup>3</sup>Ningbo Institute of Innovation for Combined Medicine and Engineering, The Affiliated Lihuli Hospital of Ningbo University, Ningbo, Zhejiang, China

**Introduction:** The natural polysaccharide-based injectable hydrogels have showed significant interest to use as 3D scaffolds for critical-sized bone defect repair.

**Methods:** Here, we incorporated ZnO nanoparticles (NPs) into a newly synthesized water-soluble phosphocreatine-functionalized chitosan (CSMP) water solution to form an injectable hydrogel (CSMP-ZnO) via supramolecular combination between phosphate groups in CSMP and Zinc in ZnO NPs.

**Results:** The phosphocreatine in this hydrogel not only provides sites to combine with ZnO NPs form supramolecular binding but also serves as the reservoir to control Zn<sup>2+</sup> release. The results show that the lyophilized CSMP-ZnO hydrogels presented a porous structure with some small holes in the pore wall, as shown by scanning electron microscopy. Rheological characterizations revealed that the mechanical properties of the hydrogels were almost maintained upon the addition of ZnO NPs. *In vitro* experiments showed that the CSMP-ZnO hydrogel exhibits excellent angiogenic and osteogenic properties compared with the CSMP hydrogel. The as-released Zn<sup>2+</sup> ions promote the high expression of osteoblast collagen 1 proteins and accelerate bone mineralization by activating the BMP2/SMAD signaling pathway. *In vivo*, the as-released Zn<sup>2+</sup> ions promote osteoblastic proliferation and the mineralization of osteoblasts inside the CSMP-ZnO scaffolds. Immunofluorescence for RUNX2, COL-1, and CD31, showed that stable vasculature could be formed inside the CSMP-ZnO scaffolds.

**Discussion:** Both the *in vitro* and *in vivo* results demonstrate that CSMP-ZnO hydrogel shows promise for bone regeneration, suggesting a new strategy for tissue engineering and regeneration in the future.

## KEYWORDS

bone regeneration, osteogenesis, phosphate-functionalized, chitosan, zinc oxide nanoparticles

## 1 Introduction

Critical-sized bone defects are usually caused by genes, infection, trauma, osteomyelitis surgery, or tumors (1, 2). Conventional treatment methods for critical-sized bone defects include autografts, allografts, xenografts, and synthetic bone grafts. However, this method is constrained by the shortage of autologous grafts, complications at the donor site, immune

rejection, and high surgical risks (3–5). To address these challenges, researchers have focused on newer materials, which can produce better results, reduce costs, and overcome problems associated with existing grafts. Bone regenerative medicine has been viewed as a promising alternative to conventional bone grafts (6, 7). Over the past decades, various approaches for bone regeneration have been studied, including tissue engineering, biomaterials, and stem cells (8–10). Among the synthetic biomaterials, hydrogels comprising natural or synthetic polymers, which exhibit excellent mechanical properties and biocompatibility, are ideal scaffolds to emulate the extracellular materials for cell proliferation and differentiation (11, 12), and natural polymers such as polypeptides, polysaccharides, and polynucleotides have been utilized to develop hydrogels (13, 14). Despite the progress in developing hydrogels, appropriately incorporating therapeutics into hydrogels to efficiently promote bone regeneration is still challenging (15–17).

Chitosan (CS) is a natural polysaccharide derived from crustacean shells (18). CS has been widely used in bone tissue engineering due to its high biocompatibility, biodegradability, biosafety, bioactivity, antibacterial activity, nontoxicity, antimicrobial, and other properties (19). The structural similarity of CS to glycosaminoglycans, the major component of the extracellular matrix of bone, has made it a suitable scaffold material for tissue engineering. These properties make CS a promising biopolymer for various applications in the biomedical field (20). CS contains a significant amount of hydroxyl and amino groups in its molecular chain structure, making it highly susceptible to the creation of strong intramolecular and intermolecular hydrogen bonding, as well as intermolecular van der Waals forces, thereby forming a more stable and organized crystalline structure, which ultimately leads to its low solubility. Therefore, CS is not soluble in water or alkaline solutions, but in inorganic acids such as dilute hydrochloric acid and dilute nitric acid, or some organic acids. CS contains three reactive functional groups: an amino group at the C2 position, a primary hydroxyl group at C3, and a secondary hydroxyl group at C6. The solubility and functionality of CS can be improved by chemically modifying these functional groups and introducing new ones. Currently, the chemical modifications for CS include acylation, alkylation, sulfonation, esterification, etherification, carboxylation, silylation, and graft copolymerization. These methods can not only retain the original properties of CS but also form CS derivatives with different functionalities, thus expanding the scope of CS application. Integrating this polymer into the structure of various inorganic materials can boost osteoblast cell growth and facilitate bone fracture healing (21–24). One attractive and frequently used modification is the methacrylation of CS, and this CS methacrylate can be used to make the photo-cross-linkable hydrogels. In addition, phosphorylation of CS is also an appealing strategy for bone regeneration applications, as phosphate is one of the main inorganic components in the bone matrix and can chelate metallic ions such as zinc, calcium, and magnesium, thereby promoting the formation of mineral bone (25, 26).

Zinc is an essential micronutrient for the human body and participates in fundamental biological processes, including energy metabolism, enzyme activity, and protein synthesis (27, 28). In the human body, 85% of zinc is in muscles and bones. Bone tissue zinc levels increase as bone mineralization increases. Alkaline phosphatase uses zinc as a co-factor and is involved in bone mineralization (29–32). Zinc can also stimulate osteoblast proliferation and increase the

expression of osteoblast gene markers and calcium deposition in the human bone marrow mesenchymal stem cells (33–35). Cho and Kwun found that zinc induces *Runx2* through canonical BMP-2 signaling (36). Recent studies suggest that incorporating zinc into synthetic polymer scaffolds for bone tissue engineering can enhance osteoblast differentiation and accelerate bone regeneration by Zn ions (37, 38). Zinc oxide nanoparticles (ZnO-NPs) have gained increasing attention for their high biocompatibility, chemical stability, and limited side effects (39). ZnO-NPs are listed as ‘generally recognized as safe material’ by the US Food and Drug Administration which possess excellent antibacterial and osteogenic capabilities (40). Qiu et al. investigated ZnO-NPs-modified CS/borosilicate bioglass composite scaffold for inhibiting bacterial infection and promoting bone regeneration (41). Yi et al. combined ZnO with mineralized collagen scaffolds with osteoinductive properties to stimulate the recruitment and differentiation of stem cells while achieving antimicrobial activity through controlled release of zinc ions, effectively treating infectious bone defects (42). To date, ample evidence suggests that bone implant scaffolds coordinated with ZnO-NPs can enhance osteogenic abilities (43, 44). ZnO NPs also activate vascular endothelial growth factor (VEGF) expression and stimulate cell proliferation, migration, and tube formation for angiogenesis (45).

In this study, the ZnO-NPs were incorporated into the synthesized methacrylate phosphorylation-functionalized CS (CSMP) to form a novel composite hydrogel via supramolecular combination with compatible bone regenerative properties, including biocompatibility, biodegradability, swelling resistance, improved mechanical, osteogenic and angiogenic properties (Scheme 1).

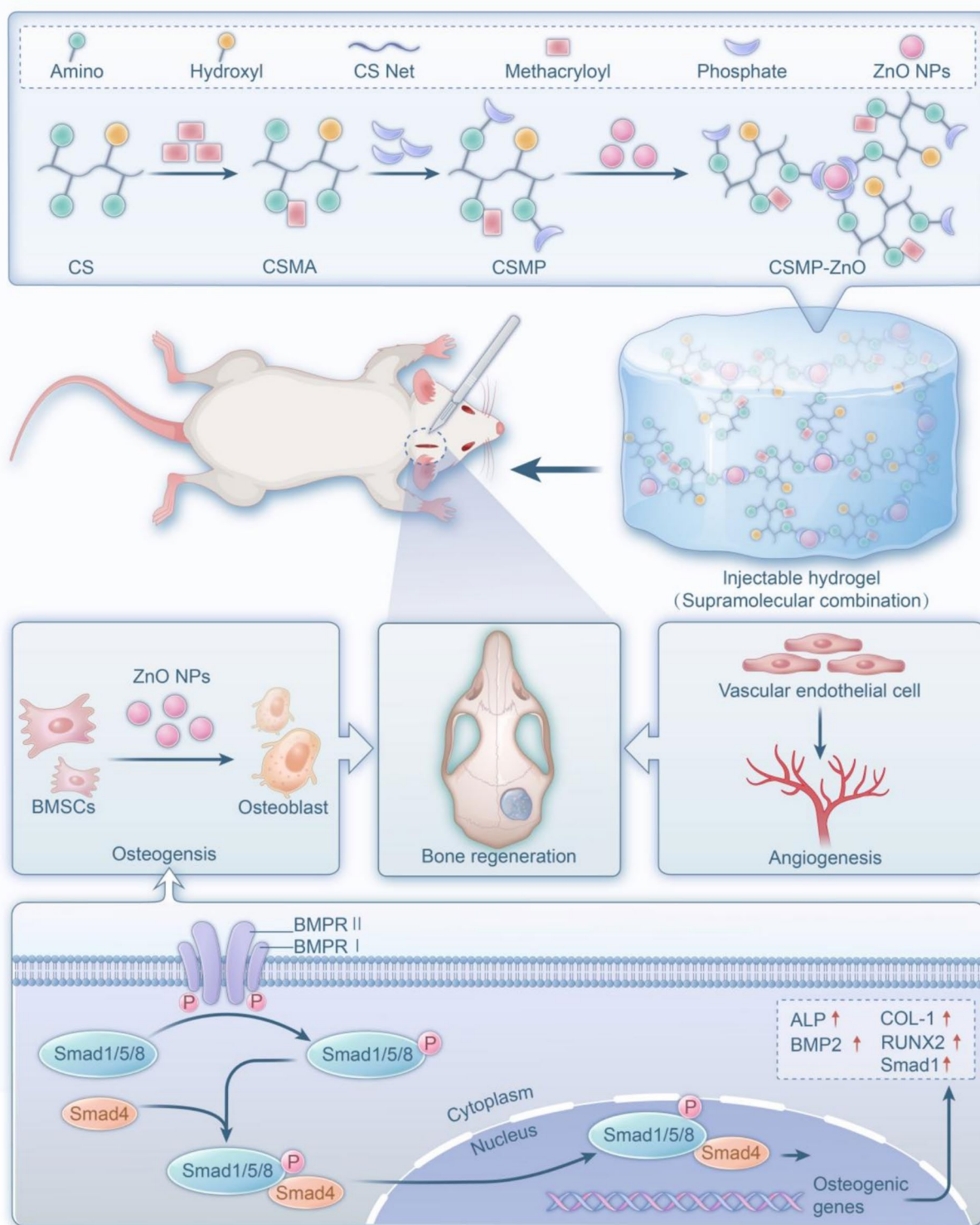
## 2 Materials and methods

### 2.1 Materials

Chitosan (Mw = 1526.500 g/mol, degree of deacetylation = 95%, viscosity = 150 mPa·s), acetate acid, 2-(N-morpholino) ethane sulfonic acid monohydrate solution (MES Solution), ZnO-NPs (Particle size: 50 ± 10 nm), acrylamide, *N,N'*-methylenebisacrylamide, 2-hydroxy-4'-(2-hydroxyethoxy)-2-methyl-propiophenone were purchased from Aladdin Biochemical Technology Co., Ltd. (Shanghai, China). Methacrylate (MA), phosphocreatine (PS), *N*-(3-dimethylamino propyl)-*N'*-ethylcarbodiimide hydrochloride, *N*-hydroxysuccinimide were purchased from Sigma-Aldrich, St. Louis, Mo, USA. Rat bone marrow-derived mesenchymal stem cells (rBMSCs) were acquired from Pricella (Wuhan, China), and human umbilical vein endothelial cells (HUVECs) were sourced from Meisen (Zhejiang, China). Dulbecco's Modified Eagle Medium (DMEM) and penicillin–streptomycin were purchased from Gibco (Thermo Fisher Scientific, USA). Fetal bovine serum (FBS) was obtained from Corning (New York, USA). The Cell Counting Kit-8 (CCK-8) reagent and Alizarin Red S (ARS) staining solution were purchased from Solarbio (Beijing, China).

### 2.2 CSMP synthesis

Three grams of CS were added to 300 mL of 1% acetate acid solution. Then 2 mL methacrylate was slowly added to the CS



SCHEME 1

Schematic diagram for the construction of the CSMP-ZnO hydrogel and its transplantation at rat cranial defects *in situ* bone regeneration.

solution. After stirring at room temperature for 12 h, a CS methacryloyl (CSMA) solution was obtained. Then, 2.4 g phosphocreatine was dissolved in 300 mL of 0.5 M 2-(*N*-morpholino) ethane sulfonic acid monohydrate solution. Then, 4.8 g *N*-(3-dimethylamino propyl)-*N'*-ethylcarbodiimide hydrochloride and

2.4 g of *N*-hydroxysuccinimide were dissolved in the PS solution. Next, the CSMA solution was added dropwise to the above solution. After reacting at room temperature for 24 h, the solution was dialyzed with deionized water (DIW) water for a week. The dialyzed solution was lyophilized to obtain the flocculent-like CSMP.

## 2.3 Composite hydrogel preparation

The CSMP was dissolved in DIW at a 20 mg/mL concentration. Subsequently, 12.5, 25, and 50 mg of ZnO-NPs were added into 50  $\mu$ L DIW. The particles were dispersed ultrasonically, and this solution was added to 5 mL of 20 mg/mL CSMP solution with rapid stirring. The concentrations of ZnO in these hydrogels were 2.5, 5, and 10 mg/mL. After mixing, the solutions were left to stand for hydrogel formation. The different concentrations of ZnO in these hydrogels were marked as CSMP-ZnO (2.5, 5, and 10). CSMP was formed using chemical cross-linking. Acrylamide 0.2 g, 2 mg *N*, *N'*-methylenebisacrylamide, and 4 mg 2-hydroxy-4'-(2-hydroxyethoxy)-2-methyl-

propiofenone were dissolved into the above-prepared CSMP solution, followed by UV irradiation for 30 min to form the CSMP hydrogel. Subsequently, the hydrogels were immersed in DIW for a week to remove any non-reacted reagents from the hydrogel, and the DIW was changed twice daily. The obtained hydrogels were stored in a refrigerator at 4 °C for further experiments.

## 2.4 Characterization

The surface morphology of hydrogels was observed using a scanning elemental microscope (SEM: GeminiSEM 360, Zeiss, Jena, Germany). The hydrogels were lyophilized and sprayed with gold. The elemental composition and distribution of the samples were detected through energy dispersion spectroscopy (EDS) in the surface mapping mode, which was equipped with the same SEM device.

The chemical composition of the hydrogels was detected using a Fourier transform infrared spectroscope (FTIR: IRTracer 100, Shimadzu, Kyoto, Japan).

The rheological experiments of the hydrogels were carried out in the oscillatory mode using a rheometer (Kinexus Lab+, NETZSCH, Germany). The hydrogels were spread on a parallel plate (25 mm), and a dynamic frequency scan in the range from 0.1 to 100 rad/s was used to record the storage and loss moduli,  $G'$  and  $G''$ . The stress amplitude and temperature were 1% and 25 °C, respectively. Each group underwent three times independent.

Cylindrical hydrogel samples (15 mm in diameter and 10 mm in height) were used for the compression test, which was performed using an electronic universal testing machine (China-UTM-5105). The compression speed was 0.5 mm/min, and the load-displacement curves were transformed into stress-strain curves. The maximum stress was taken from the turning point on the curve, and the compressive modulus was calculated from the linear range in the stress-strain curve before the turning point.

The swelling ratio of the hydrogels was measured by immersing the fabricated cylindrical hydrogels (dry weight,  $W_0$ ) in DIW at room temperature. At the set time points, the height of hydrogels was weighted ( $W_1$ ) until they were swollen. Each group underwent three times independent. The degradation rate formula for hydrogels is as follows:

$$\text{Swelling ratio (100\%)} = \frac{W_1}{W_0} \times 100\%$$

The *in vitro* degradation behavior of the hydrogels was evaluated by soaking the lyophilized hydrogels in phosphate-buffered saline

(PBS, Pricella, Wuhan, China) in a static state at 37 °C for up to 28 days, and the PBS solutions were changed every 2 days. In brief, the lyophilized hydrogels (weighted as  $W_0$ ) were immersed in PBS at 37 °C. At set time points (days 1, 3, 5, 7, 14, and 21), the hydrogels were lyophilized and weighted as  $W_1$ . Each group underwent three times independent. The degradation rate formula for hydrogels is as follows:

$$\text{Degradation rate (100\%)} = \frac{W_0 - W_1}{W_0} \times 100\%$$

For zinc ion release, the hydrogel scaffolds were soaked in a centrifuge tube with 5 mL PBS solution. At different time points (days 1, 3, 5, 7, 14, 21, 28). The zinc ion concentration in these collected PBS solutions was detected using inductively coupled plasma atomic emission spectroscopy (ICP-AES, Agilent 5,800, USA). Each group underwent three times independent.

The extraction of CSMP, CSMP-ZnO (2.5), CSMP-ZnO (5), and CSMP-ZnO (10) scaffolds was prepared as previously described by the International Organization for Standardization method (ISO10993-12) (46). Briefly, the scaffolds were incubated in a culture medium for 24 h at a mass/volume ratio of 100 mg/mL at 37 °C. After 24 h, the supernatants were collected and filtered through a sterilized 0.22 mm Millipore (Biosharp, China) and stored at 4 °C (ISO 10993-12) for further use.

## 2.5 Cell culture and cell seeding

Rat bone marrow-derived mesenchymal stem cells (rBMSCs, Pricella, Wuhan, China) and human umbilical vein endothelial cells (HUVECs, Meisen CTCC, Zhejiang, China) were, respectively, cultured in  $\alpha$ -MEM and endothelial cell medium (ECM) supplemented with 10% fetal bovine serum (FBS, Corning, USA) and 1% penicillin-streptomycin (Gibco, USA) solution in a humidified incubator with 5% CO<sub>2</sub> at 37 °C. The medium was changed every 2 days. When cell growth reached 80–90% confluence, the cells were digested with trypsin (Gibco 25,200,056, USA). The cell suspension was centrifuged to remove the medium after terminating the digestion by adding the cell medium. The cells were resuspended in a new cell culture medium, and the suspending solution was seeded into a plate for subsequent experiments.

## 2.6 Cell toxicity and proliferation

To study the effect of hydrogels on the proliferation and viability of rBMSCs and HUVECs,  $5 \times 10^3$  rBMSCs and HUVECs were seeded in a 24-well plate and incubated in the scaffold extraction medium or standard medium (control) for 1, 3, and 5 days. Subsequently, the cell viability was assessed using the cell counting kit-8 (CCK-8, Biosharp, China). The absorbance values at 450 nm were measured using a microplate reader (Thermo Fisher Scientific, USA). Each group underwent three times independent.

Live/dead staining tests were conducted to evaluate the *in vitro* cytotoxicity of the hydrogels.  $1 \times 10^5$  rBMSCs and HUVECs were seeded in a 24-well plate and incubated in the scaffold extraction medium or standard medium (control) for 1, 3, and 5 days. The cells were immersed in PBS containing 4 mM calcein acetoxyethyl ester

(AM) and 16 mM propidium iodide (PI) for 30 min. Dead cells (PI, red) and live cells stained with calcein (AM, green) were observed with a fluorescence microscope (Leica DMi8, Germany).

## 2.7 In vitro osteogenic differentiation of BMSCs

### 2.7.1 Extracellular matrix mineralization assay and alkaline phosphatase (ALP) activity assay

The osteogenic differentiation culture medium was prepared by adding 10 mM  $\beta$ -sodium glycerophosphate (Aladdin Chemistry), 50  $\mu$ M L-ascorbic acid (Aladdin Chemistry), and  $10^{-7}$  M dexamethasone (Aladdin Chemistry) to the standard culture medium. This medium promotes ALP activity and calcium phosphate deposition. About  $1 \times 10^5$  rBMSCs were seeded on a 24-well plate and then incubated in extractions prepared from osteogenic differentiation culture medium for 14 and 21 days, and the medium was changed every 2 days. Next, the cells were fixed with 4% paraformaldehyde (Solarbio, Beijing, China). Then, the samples were washed thrice with PBS for 10 min each time. The samples were stained using an ALP staining kit (Beyotime, Shanghai, China) and an Alizarin Red staining kit (ARS, Solarbio). On days 14, ALP activity was measured using ALP activity assay kit (Elabsience, Wuhan, China). Each group underwent three times independent.

### 2.7.2 Quantitative real time-polymerase chain reaction (qRT-PCR)

$4 \times 10^5$  rBMSCs were seeded in a 6-well plate for 24 h and grouped into control, CSMP, and CSMP-ZnO groups. These samples were then incubated in the extracts prepared from the osteogenic differentiation culture medium for 7 days. Following that, the extraction solution of the scaffold material was changed every 2 days. Total RNA for each sample was extracted according to the protocol of the RNA extraction kit (TransGen, Beijing, China). The extracted RNA was then reverse-transcribed to complementary DNA (cDNA) with the RT reagent kit (PrimeScript™ RT Master Mix, TransGen), and the cDNA was used for qRT-PCR assay (Thermo Fisher Scientific, QuantStudio 5, USA). The mRNA levels of osteogenic genes recombinant bone morphogenetic protein 2 (*BMP2*), recombinant runt related transcription factor 2 (*RUNX2*), collagen type-I (*COL-1*), SMAD family member 1 (*Smad1*), and *ALP* were evaluated and were normalized with the internal control glyceraldehyde-3-phosphate dehydrogenase (*GAPDH*). Each group underwent three times independent. The PCR primers were designed to amplify the interest genes, as shown in [Table 1](#).

### 2.7.3 Western blot (WB) analysis

WB was employed to verify the expression of osteoblast differentiation proteins. The osteoblast-associated proteins COL-1, BMP2, RUNX2 expressions were measured. Around  $4 \times 10^5$  rBMSCs were seeded in a 6-well plate for 24 h and grouped into control, CSMP, and CSMP-ZnO groups. These samples were then incubated in the extracts prepared from the osteogenic differentiation culture medium for 7 days. Following that, the extraction solution of the scaffold material was changed every 2 days. The radioimmunoprecipitation assay (RIPA) lysis buffer solution (Solarbio) was used to soak the cells for 30 min, and the lysed samples were collected in a 1.5 mL microcentrifuge tube. These samples were centrifuged at 12,000 rpm

TABLE 1 PCR primers designed to amplify the genes of interest.

Gene	Primer sequences (5'-3')
COL-1	F:5'- GCGTAGCCTACATGGACCAA -3'
	R:5'- AAGTTCGGGTGTGACTCGTG -3'
RUNX-2	F:5'- TCGGAGAGGTACCAGATGGG -3'
	R:5'- TGAAACTCTTGCTCGTCCG -3'
BMP-2	F:5'- GACTGCGGTCTCCTAAAGGTCG -3'
	R:5'- CTGGGGAAGCAGCAACTA -3'
SMAD1	F:5'- GGTGACTGGGAACGGATCG -3'
	R:5'- CCCAGTTAGCACCCGGCTC -3'
ALP	F:5'- TGCAGGATCGGAACGTCAAT -3'
	R:5'- GAGTTGGTAAGCAGGGTCC -3'
VEGF	F:5'- ACAATGTGAATGCAGACCAAAG -3'
	R:5'- GGAGGCTCCAGGCATTAGA -3'
FGF2	F:5'- GCGACCCTCACATCAAGCTA -3'
	R:5'- AGCCAGGTAACGGTTAGCAC -3'
GAPDH	F:5'- CCGCATCTTCTGTGCAGTG -3'
	R:5'- CGATACGGCCAATCCGTTTC -3'

for 15 min, and the supernatants were collected. A bicinchoninic acid protein assay Kit (Solarbio) was used to detect the total protein concentration. The samples were loaded in sodium dodecyl sulfate-polyacrylamide gel electrophoresis (SDS-PAGE) gel for electrophoresis and transferred to polyvinylidene difluoride (PVDF; Solarbio) membranes. After blocking in 5% milk for 1 h, the membranes were incubated with primary antibodies ([Supplementary Figure S1](#)) at 4 °C overnight and washed with tris-buffered saline with tween-20 (TBST; Solarbio) three times. These membranes were then incubated with secondary antibodies (Proteintech, USA). Finally, the blotting results were checked by the imaging system (Tanon 5,200, Shanghai, China). Each group underwent three times independent.

### 2.7.4 Immunofluorescence staining

$4 \times 10^5$  rBMSCs were seeded in a 6-well plate for 24 h and grouped into control, CSMP, and CSMP-ZnO groups. Then, these samples were incubated in the extracts prepared from the osteogenic differentiation culture medium for 7 days, and the medium was changed every 2 days. The specimens from each group were washed with PBS solution three times and fixed with 4% paraformaldehyde for 20 min, then washed thrice with PBS. Subsequently, after incubation with 0.5% Triton X-100 (Beyotime) in PBS for 20 min, the specimens were blocked in PBS containing 1% bovine serum albumin (BSA; Solarbio) for 30 min. Next, these samples were incubated with the primary antibodies anti-COL1 (1:200, Affinity, USA), anti-ALP (1:200, Affinity, USA) overnight at 4 °C. The secondary antibodies were then conjugated with fluorescein isothiocyanate (FITC) or tetramethylrhodamine isothiocyanate (TRITC) and incubated at 37 °C for 1 h. The nucleus was stained with 4,6-diamino-2-phenyl indole (DAPI). The images were observed and collected with a fluorescence microscope (Leica DMi8, Germany).

## 2.8 *In vitro* angiogenic differentiation of HUVECs

### 2.8.1 Scratch assay

The effect of scaffolds on HUVECs migration activity was studied using the scratch assay. Briefly,  $6 \times 10^4$  HUVECs were cultured in a 6-well plate for 12 h to allow the cells to fully cover the bottom of the plate, and the scratch was made with a 200  $\mu$ L pipette head. Each well was filled 2 mL of sample extracts. After 24 h of co-culture, the healing of the scratch area was observed under an optical microscope (CKX3-SLP, Olympus, Tokyo, Japan). Each group underwent three times independent.

### 2.8.2 Transwell assay

Transwell plates with a membrane pore size of 8  $\mu$ m (Corning, NY, USA) were involved to conduct the transwell assay, where each lower chamber was loaded with scaffolds extraction.  $4 \times 10^5$  HUVECs were seeded into the upper chamber of 24-well transwell plates and allowed for 24 h migration. Cells migrated from the upper chamber to the bottom of each well were then immersed in 4% paraformaldehyde for 30 min and stained with a 0.5% crystal violet solution for 30 min. Finally, three randomly selected visual fields and corresponding images were taken and analyzed with an optical microscope (CKX3-SLP, Olympus, Tokyo, Japan). Each group underwent three times independent.

### 2.8.3 Tube formation assay

To detect the tube formation ability of the scaffolds, Matrigel (Corning, New York, USA) was spread on the bottom of a 24-well plate. Added  $4 \times 10^5$  HUVECs within 1 mL of sample extracts into each well. After 6 h incubation, tube formation was observed under an optical microscope (CKX3-SLP, Olympus, Tokyo, Japan). Each group underwent three times independent. Further quantitative analysis of the number of joint and total tube length was conducted with ImageJ software.

### 2.8.4 qRT-PCR assay

HUVECs were seeded at  $4 \times 10^5$  cells/mL on 6-well plates for 1 day, then the medium was replaced with sample extracts and continue to culture for 7 days. The experiment procedure has been described in 2.6.2. The expression of classic angiogenic related genes, such as vascular endothelial growth factor (*VEGF*), and fibroblast growth factor 2 (*FGF2*) were analyzed. Each group underwent three times independent. The primer sequences are listed in Table 1.

### 2.8.5 WB assay

HUVECs were seeded at  $4 \times 10^5$  cells/mL on 6-well plates for 1 day, then the medium was replaced with sample extracts and continue to culture for 7 days. The experiment procedure has been described in 2.6.3. The expression of classic angiogenic related protein, such as vascular endothelial growth factor (*VEGF*), and fibroblast growth factor 2 (*FGF2*) were analyzed (Supplementary Figure S1). Each group underwent three times independent.

## 2.9 *In vivo* animal study

All the animal feeding and surgical procedures complied with the relevant laws and were authorized by the Ethics Committee of Ningbo

University. Twelve 6-week-old female Sprague–Dawley (SD) rats were purchased from the Laboratory Animal Center of Ningbo University of China. They were randomly divided into control group, CSMP group, and CSMP-ZnO group, with nine rats in each group. All the animals were anesthetized intraperitoneally with 3% pentobarbital sodium (30 mg/kg). Under sterile conditions, a midline sagittal incision in the scalp was made to expose the parietal bone, and the pericranium was removed by blunt scraping. A critical-size (5 mm in diameter) defect was created below the right side of the crown bone. Bone defects were washed with sterile normal saline, and the hydrogel of each group was implanted into the defect area. The group without any hydrogel scaffold served as the negative control group. After 4- and 8-week implantation periods, these rats were sacrificed with excessive anesthesia. The whole skull was obtained, and the bone defects were investigated using a micro-CT system (Venus<sup>®</sup> Micro CT VNC-102, Jiangsu, China). New bone volume (BV), new bone volume/tissue volume (BV/TV) ratios, and trabecular bone number (Tb.N) were calculated using appropriate analysis software. Each group underwent three times independent. Then, these samples were fixed in a 4% paraformaldehyde solution for 7 days, after which the tissues were decalcified by being immersed in 10% ethylenediaminetetraacetic acid (EDTA, Codow, China) solution for 4 weeks. Subsequently, the tissues were embedded in paraffin. The cranial cross sections in the central area of the defect were cut at 5  $\mu$ m for hematoxylin and eosin (H&E), Masson, and immunohistochemical staining for runt related transcription factor 2 (RUNX2, 1:100, AF5186, Affinity), COL-1 (1:100, AF7001, Affinity) and CD31 (1:100, AF6191, Affinity).

## 2.10 Statistical analysis

SPSS 22.0 was used for statistical analysis. The experimental data were expressed as mean  $\pm$  SD. A one-way ANOVA was used to compare groups, and the LSD method was used for multiple comparisons.  $p < 0.05$  was considered statistically significant.

## 3 Results

### 3.1 Rheological properties of the hydrogel

We carried out rheological experiments to confirm the formation of the hydrogels and characterize their mechanical properties. According to the frequency-dependent oscillatory shear model, the elastic moduli  $G'$  for all hydrogels were 10-fold greater than their corresponding viscous moduli  $G''$  (Figures 1b,c), indicating the formation of hydrogels. Upon reaching the plateau, all the hydrogels displayed a storage modulus  $> 1$  kPa, indicating their moderate mechanical characteristics and potential use as scaffolds for bone regeneration. The addition of ZnO-NPs to CSMP hydrogel resulted in a slight decline in mechanical properties, primarily due to the varied ways of hydrogel formations. Among these, CSMP-ZnO (5) had the highest  $G'$  value.

### 3.2 Surface characterization of hydrogels

The surface morphology of lyophilized hydrogels was observed using SEM (Figure 1a; Supplementary Figures S2a,b). All the hydrogels

presented a porous structure, and the pore diameter ranged between 50 and 100  $\mu\text{m}$ . The energy-dispersive X-ray spectrometry (EDS) analyses confirmed the homogeneous distribution of C, N, O, P, and Zn elements in the CSMP-ZnO hydrogel (Supplementary Figure S3).

The chemical composition and bonding state of hydrogels were confirmed through FTIR assessments. Based on the FTIR spectra in (Figure 1f), the characteristic peaks of stretching C–N ( $1316.2\text{ cm}^{-1}$ ), O–H ( $1409.7\text{ cm}^{-1}$ ), N–H bending vibration ( $1605.8\text{ cm}^{-1}$ ), and  $\text{PO}_4^{3-}$  group ( $1074.5\text{ cm}^{-1}$ ) bonds from CS derivatives of CSMP were detected for CSMP and CSMP-ZnO (5) hydrogels. Meanwhile, we can observe the C=O ( $1653.7\text{ cm}^{-1}$ ) stretching corresponding to the amide bond produced by the CS modification reaction. However, only the characteristic peak for ZnO–P was observed in the CSMP-ZnO (5) sample. The distinctive peak of ZnO–P signifies the combination of ZnO–NPs and phosphate groups in CSMP.

### 3.3 Compressive properties of hydrogels

The compressive stress–strain curves of hydrogels were investigated, and the results are shown in (Figures 1d,e). For maximum compressive strength, CSMP was  $22.39 \pm 4.33\text{ KPa}$ , CSMP-ZnO (2.5) was  $50.55 \pm 6.37\text{ KPa}$ , CSMP-ZnO (5) was  $120.48 \pm 14.24\text{ KPa}$ , and CSMP-ZnO (10) was  $88.14 \pm 11.24\text{ KPa}$ .

### 3.4 Swelling property of hydrogels

Swelling is an essential characteristic of hydrogels to promote tissue regeneration. The swelling of hydrogels expands the hydrogel volume, weakens their mechanical properties, and oppresses the surrounding tissue, impeding normal metabolism and, consequently, impacting tissue regeneration. Therefore, anti-swelling hydrogels are more desirable for tissue regeneration (47). The swelling property of lyophilized hydrogels was investigated by immersing them in DIW until they swelled (600 min) (Figure 1g), in the initial immersion (0–150 min), the swelling ratio for all the hydrogels was dramatically increased. Over time, the increase in the ratio for all the hydrogels slowed down until they reached the final swollen state. Similarly, CSMP hydrogels showed higher swelling ratios, having the largest swelling ratio, during the entire immersion period compared to CSMP-ZnO (2.5, 5, and 10) hydrogels, and the CSMP hydrogel presented the largest swelling ratio. As ZnO levels rose, the CSMP-ZnO group's swelling rate reduced, suggesting that CSMP-ZnO with higher ZnO concentrations exhibited superior anti-swelling effects.

### 3.5 *In vitro* immersion degradation behavior of hydrogels

The biodegradability and degradation behaviors of biomaterials are significant for tissue regeneration. Ideal bone repair materials

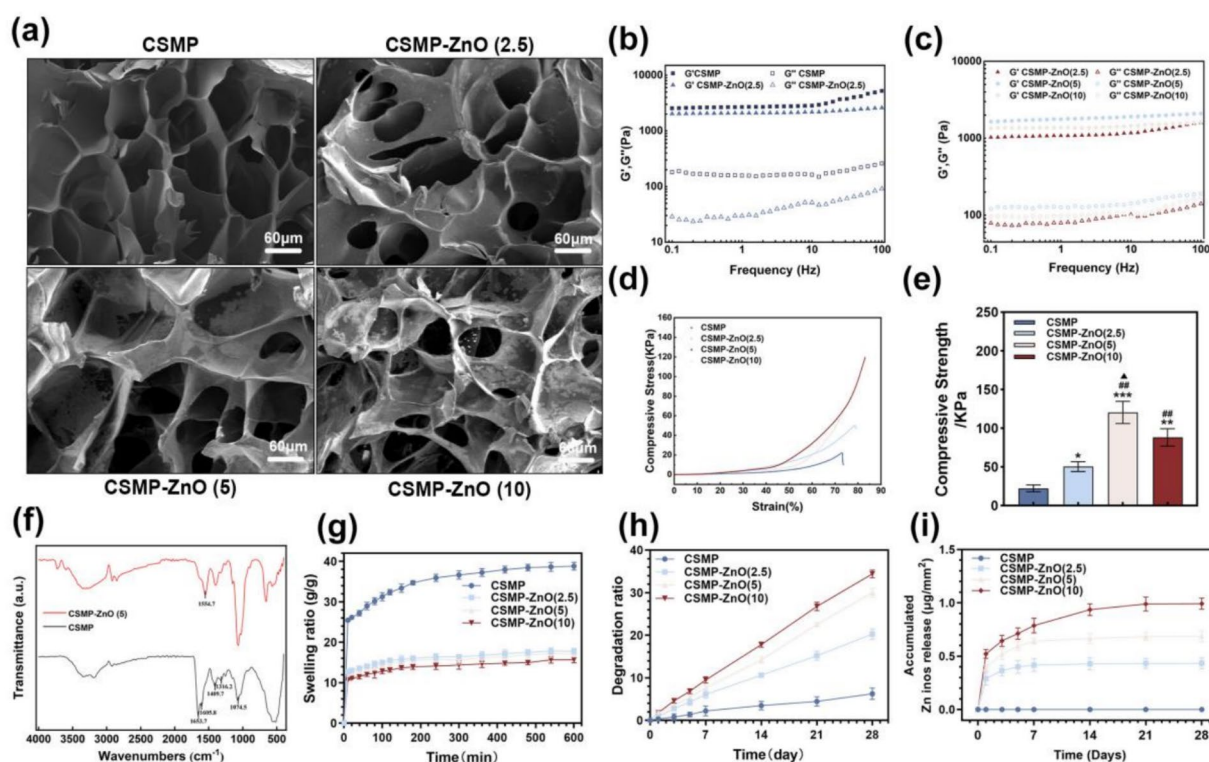


FIGURE 1

Characterization for hydrogels: (a) SEM images; (b,c) frequency sweeping of elastic moduli  $G'$  and viscous moduli  $G''$  for hydrogels from 0.1 to 100 Hz under 1% strain at  $37^\circ\text{C}$ ; (d) stress–strain curves; (e) maximum compressive strength; (f) FTIR spectra; (g) swelling ratio of lyophilized hydrogels in DI water as a function of immersion time; (h) mass remaining ratio of hydrogels; (i) accumulative  $\text{Zn}^{2+}$  release in the hydrogel scaffolds. Data are presented as mean values  $\pm$  SD ( $n = 3$ ). \*Compared with CSMP. #Compared with CSMP-ZnO(2.5).  $\blacktriangle$ Compared with CSMP-ZnO (10). \* $p < 0.05$ , \*\* $p < 0.01$ , \*\*\* $p < 0.001$ ; # $p < 0.05$ , ## $p < 0.01$ , ### $p < 0.001$ ;  $\blacktriangle p < 0.05$ ,  $\blacktriangle\blacktriangle p < 0.01$ ,  $\blacktriangle\blacktriangle\blacktriangle p < 0.001$ .

should be fully biodegradable, and the degradation rate should match the bone tissue regeneration rate (48). Therefore, the *in vitro* immersion degradation behavior of the hydrogels was investigated (Figure 1h). The experiment demonstrated the degradation rate of hydrogels when they were immersed in PBS under agitation at 37 °C for 28 days, with periodic measurements taken. As the immersion time increased, the mass of all hydrogels decreased. After 28 days, the CSMP-ZnO hydrogels presented a larger mass decrease than CSMP. As the content of ZnO increases, the degradation ratio of ZnO hydrogel increased. Our study found that CSMP-ZnO (10) had the highest degradation rate. We speculate that the mass loss of CSMP-ZnO hydrogels might be attributed to the degradation of ZnO.

Based on the release of Zn ions in Figure 1i, these ions were largely released in the initial stage for all ZnO-incorporated CSMP hydrogels; with increasing immersion time, the Zn ion release rate decreased. As expected, more ZnO-incorporated hydrogels released more Zn ions during the immersion period. The release of Zn ions in CSMP-ZnO (10) hydrogel presented the largest Zn ion release.

### 3.6 The proliferation and viability of the rBMSCs and HUVECs

Calcein-AM/PI (live/dead) staining was performed to explore the biocompatibility of the hydrogels by detecting the viability of co-culture rBMSCs and HUVECs at day 1, 3, and 5, in which living cells were stained with green while dead cells were stained with red. All hydrogels showed excellent biocompatibility for both rBMSCs and HUVECs, as hardly any dead cells could be seen in fluorescence micrographs (Figures 2a,b). Moreover, enhanced HUVECs proliferation was observed in the hydrogels containing Zn ions (Figure 2b). The excellent biocompatibility of these hydrogels was also confirmed by quantitative analysis of CCK-8 assay (Figures 2c,d). It was found that higher OD values of HUVECs was observed in CSMP-ZnO (2.5, 5, 10) group on days 3, and 5 compared with the CSMP group, indicating that the introduced Zn ions possess the ability to promote the proliferation of HUVECs.

### 3.7 *In vitro* osteogenic properties of hydrogel scaffolds

To further verify the bone-inducing and mineralizing abilities of each group of scaffolds, *in vitro*, ALP staining, ALP activity assay, and ARS staining were performed. From the ALP staining images (Figure 3a), we observed that on day 14, all the hydrogel samples' staining became dark. Among the composite hydrogels, CSMP-ZnO (5) exhibited an intensely dark color. The ALP activity is represented in (Figure 3c). Compared to other groups, the cells in the CSMP-ZnO (5) scaffolds showed the highest activity. The CSMP scaffold group had higher activity than the control group but was less than that of the CSMP-ZnO (5) scaffold group. To identify and estimate the formation of calcium nodules in the ECM of rBMSCs after exposure to all the hydrogels for 21 days. ARS demonstrated similar results to ALP staining and activity (Figure 3b). CSMP-ZnO (5) hydrogels showed a larger and deeper red area than other hydrogels. The CSMP-ZnO (5) hydrogel was chosen for the subsequent experiments for the following

reasons: (1) CSMP-ZnO (5) exhibits excellent rheological properties, compressive properties, anti-swelling effects, and degradation; (2) CSMP-ZnO (5) demonstrates favorable biocompatibility.

It was observed that CSMP-ZnO scaffolds can promote osteoblast differentiation. Hence, we further explored the molecular mechanism of the above phenomenon. By employing WB and qRT-PCR, the osteoblast-specific proteins (Figures 3d–g) and genes (Figures 3h–l) were detected. Compared to the control group, the osteoblast-related proteins (COL-1, RUNX2, and BMP2) were higher in the CSMP and CSMP-ZnO. Similarly, the gene expression (COL-1, RUNX2, BMP2, Smad1, and ALP) in the CSMP and CSMP-ZnO groups was also higher, with the CSMP-ZnO group showing superior osteogenic properties. COL-1 is the major component of the organic matrix of bone, which promotes calcium and phosphorus deposition and accelerates new bone tissue calcification (49). RUNX2 is a fundamental transcription factor for bone development and regulating the differentiation of mesenchymal stem cells into osteoblasts. In immature osteoblasts, RUNX2 regulates the expression of bone matrix protein genes, including COLA1 and COLA2, and induces osteoblast maturation (50). BMP2 and Smad1 are target proteins in the classic osteoblast differentiation pathway, stimulating the mesenchymal stem cells to differentiate into osteoblasts (51). We speculated that the Zn<sup>2+</sup> ions from the CSMP-ZnO scaffolds promoted osteoblast differentiation by activating the BMP2–Smad1 signaling pathway. Regarding osteoinductive genes and proteins, the osteoinductive ability is the control < CSMP < CSMP-ZnO. Simultaneously, the CSMP-ZnO scaffold exhibited a more pronounced impact on enhancing osteoblast differentiation, possibly attributable to the synergistic influence of Zn<sup>2+</sup>. In addition, the protein levels of COL-1 and ALP were visualized using a fluorescence microscope. The immunofluorescence images showed the augmented expressions of COL-1 (Figures 4a,c) and ALP (Figures 4b,d) in the CSMP-ZnO group compared to those in the CSMP hydrogel and control groups.

### 3.8 *In vitro* angiogenic properties of hydrogel scaffolds

To determine the *in vitro* angiogenic properties of the hydrogels, scratch assay, transwell assay, and tube formation assay were performed using HUVECs. As shown in Figure 5a, scratches with the same width were made on the bottom of each well at 0 h. After 24 h healing, significant thinner scratches were observed in CSMP-ZnO groups while much wider scratches remained in the Control and CSMP groups, suggesting that the addition of ZnO in hydrogels could significantly accelerate cell migration. Further quantitative analysis showed that the migration ratio of HUVECs in CSMP-ZnO group was 1.6-fold higher than that in CSMP group (Figure 5b).

Another transwell experiment using crystal violet staining to characterize permeabilized cells was performed to confirm the effect of hydrogels on cell migration. As presented in Supplementary Figure S4, significantly more migrated cells were observed in the CSMP-ZnO groups compared with CSMP and control groups. Therefore, it suggests that the ions released could promote cell migration.

To further verify the angiogenesis properties of different hydrogels, the matrigel experiment (tube formation assay) that can directly reflect the vascularity generation level was conducted. In Figure 5c,

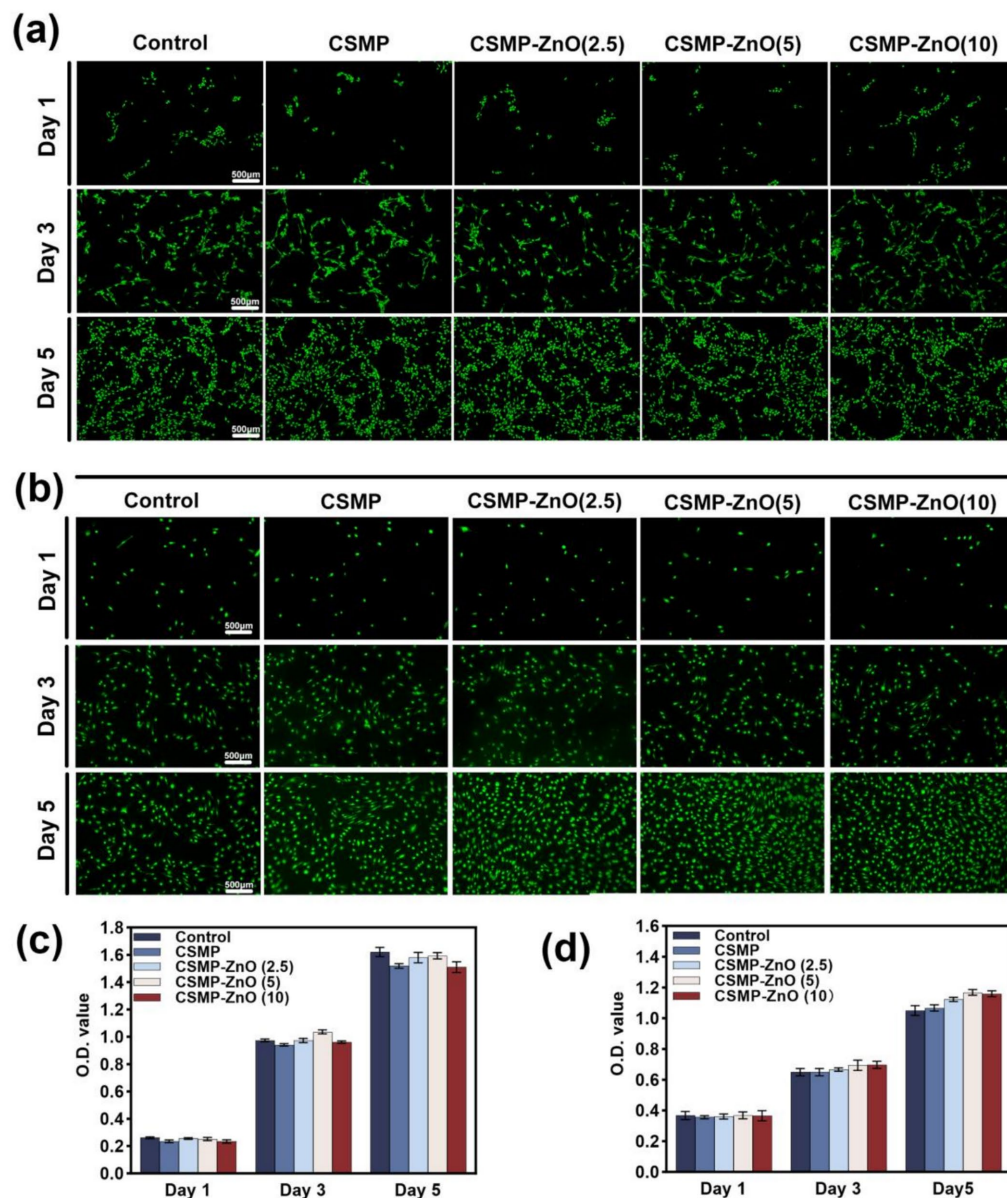


FIGURE 2

The biocompatibility of hydrogels for rBMSCs evaluated by (a) Calcein-AM/PI (live/dead) staining and (c) CCK-8 assay. The biocompatibility of hydrogels for HUVECs evaluated by (b) Calcein-AM/PI (live/dead) staining and (d) CCK-8 assay. Data are presented as mean values  $\pm$  SD ( $n = 3$ ).

\*Compared with control. #Compared with CSMP. \* $p < 0.05$ , \*\* $p < 0.01$ , \*\*\* $p < 0.001$ .

significantly more tube structures were observed in CSMP-ZnO groups. Further quantitative results demonstrated 1.37-fold and 1.32-fold increase of junction number and total length in CSMP-ZnO group compared with CSMP group (Figures 5d,e). Moreover, the expression of angiogenic genes (*VEGF* and *FGF2*) and proteins (*VEGF* and *FGF2*) of HUVECs cultured with different hydrogels was detected. Similarly, significantly higher angiogenic genes (1.22-fold for *VEGF* and 2.28-fold for *FGF2*) (Figures 5f,g) and proteins expression (1.85-fold for *VEGF* and 1.34-fold for *FGF2*) (Figures 5h-j) were observed in CSMP-ZnO and CSMP groups, indicating their better angiogenic properties. In conclusion, the CSMP-ZnO hydrogel could accelerate cell migration, activate angiogenic gene expression, and thus promote angiogenesis performance of hydrogels.

### 3.9 Osteogenic activities of the hydrogel scaffolds *in vivo*

The hydrogels were implanted into the 5 mm rat cranial defects to investigate their *in vivo* osteogenic properties. Following 4 and 8 weeks of implantation, the cranial bone was collected for micro-CT analysis to evaluate the newly formed bone. Based on the micro-CT results from (Figure 6a), a larger area of regenerated bone was observed for the CSMP-ZnO (5) hydrogels at 4 weeks than the CSMP and control groups. As the implantation period increased, the regenerated bone area increased for CSMP-ZnO (5) hydrogels, but the control group presented no significant increase. The statistical analysis results for BV, BV/TV, and Tb.N are shown (Figures 6b-d). At 4 weeks, the BV and

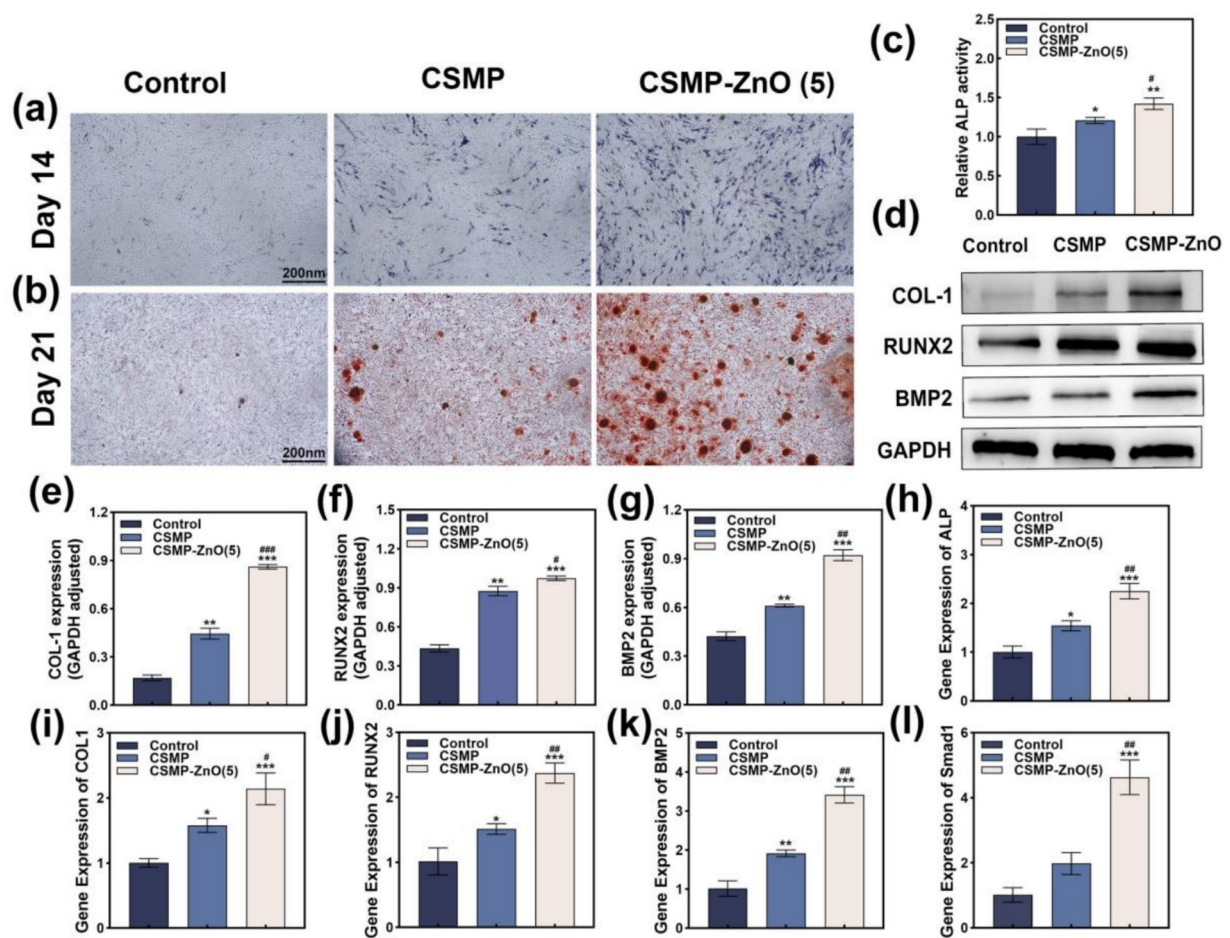


FIGURE 3

The osteogenic properties of hydrogels. (a) Alkaline phosphatase and (b) Alizarin red S staining of rBMSCs cultured with blank control, CSMP and CSMP-ZnO (5) scaffolds extraction medium. (c) Quantitative analysis results of Alkaline phosphatase. (d–g) Osteogenic proteins (COL-1, RUNX2, BMP2) expression of rBMSCs cultured with blank control, CSMP and CSMP-ZnO (5) scaffolds extraction medium evaluated by Western blot. (h–l) Osteogenic gene (COL-1, RUNX2, BMP2, Smad1, ALP) expression of rBMSCs cultured with blank control, CSMP and CSMP-ZnO (5) scaffolds extraction medium evaluated by qPCR. Quantitative analysis results of osteogenic proteins expression of rBMSCs using ImageJ. Data are presented as mean values  $\pm$  SD ( $n = 3$ ). \*Compared with control. #Compared with CSMP. \* $p < 0.05$ , \*\* $p < 0.01$ , \*\*\* $p < 0.001$ ; # $p < 0.05$ , ## $p < 0.01$ , ### $p < 0.001$ .

BV/TV of regenerated bone for CSMP-ZnO (5) were higher than the CSMP and control groups, and Tb. N also showed a similar tendency. The Tb. N of regenerated bone for CSMP-ZnO (5) hydrogel was higher than in other groups. Over time, this tendency remained the same.

H&E and Masson's trichrome staining further verified the histological formation and maturity of new bone (Figure 7a). The H&E staining revealed that the CSMP-ZnO (5) hydrogel group exhibited significant new bone and blood vessel repair at the bone defect site, with no remaining undegraded implantation. As shown in Supplementary Figure S5, Supporting Information, no difference was observed in the heart liver, spleen, kidney and lung tissue sections between 0-week, 4-week, 8-week after sample implantation, confirming the excellent biocompatibility of CSMP-ZnO. Significantly, the growth of new blood vessels was also seen in the CSMP-ZnO (5) group. After 4 weeks of implantation, the stained area was larger for CSMP-ZnO (5) than CSMP. When the implantation period increased, the stained areas for all hydrogels increased significantly for CSMP-ZnO (5) hydrogels. The CSMP-ZnO (5) implanted area presented more new bone area than the other two groups. After 8 weeks of implantation, in the CSMP-ZnO (5) group, the new bone

regeneration fully repaired the bone defect site, generation mature bone tissue and vascularization. In the regenerated tissue, there was superior columnar organization and integration compared to other groups. Furthermore, the CSMP-ZnO (5) hydrogel contains abundant collagen fibers. Compared to the CSMP hydrogel, more new cells, dense collagen, and new vasculature were observed at the center of the bone defect site in the CSMP-ZnO (5) hydrogel group. These results suggest that CSMP-ZnO (5) hydrogel promotes osteogenesis and angiogenesis and inhabits fibrous tissue growth.

Masson's staining was used to analyze the collagen and newly formed bone. Masson's trichrome staining shows that mature bone matrix (collagenous tissue) is stained blue, and muscle tissues and red blood cells are also stained red. Only a small amount of new, immature bone matrix (mainly including muscle fibers and partially collagen) can be observed in the control group. In contrast, the newly formed collagen (blue) and blood vessels (red) were obvious in CSMP and CSMP-ZnO (5) hydrogels after 4 weeks, similar to the results of H&E staining. CSMP-ZnO (5) hydrogel group has abundant and denser collagen and blood vessels. The control group exhibited a limited amount of mature bone and newly formed blood vessels at the defect

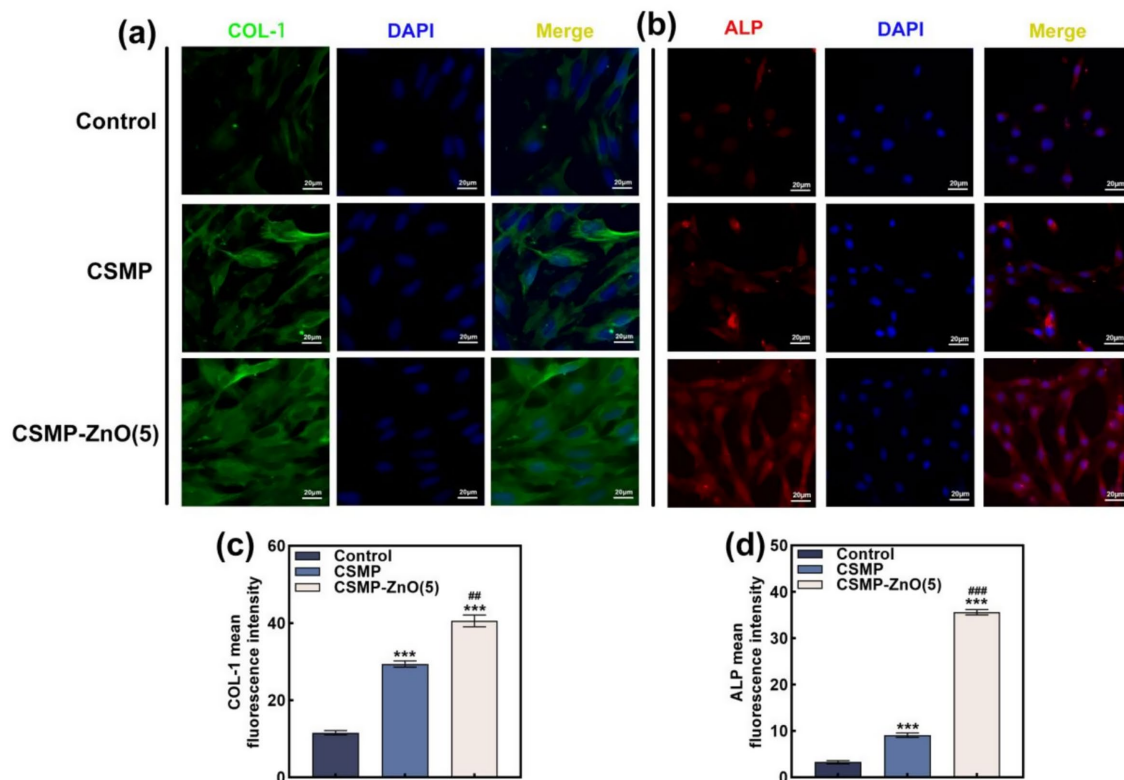


FIGURE 4

Representative immunofluorescence images of rBMSCs cultured with blank control, CSMP and CSMP-ZnO (5) scaffolds extraction medium: (a) COL-1 and (b) ALP. (c,d) Quantitative analysis of IF for COL-1 and ALP. Data are presented as mean values  $\pm$  SD ( $n = 3$ ). \*Compared with control. #Compared with CSMP. \* $p < 0.05$ , \*\* $p < 0.01$ , \*\*\* $p < 0.001$ ; # $p < 0.05$ , ## $p < 0.01$ , ### $p < 0.001$ .

site after 8 weeks. In contrast, the CSMP-ZnO (5) group exhibited a substantial amount of mature bone matrix and a greater number of blood vessels. The well-arranged collagens were stained a deep blue color, and more blood vessels were growing at the bone defect site, indicating that CSMP-ZnO (5) hydrogel can osteogenesis and angiogenesis. H&E and Masson's trichrome staining showed no inflammatory response or necrosis in the newly formed fibrous tissue in all the groups. However, dense, mature, freshly formed fibrous tissue and neovascularization were observed in the CSMP-ZnO (5) group, suggesting that blood supply can promote fibrous tissue formation.

The results were confirmed by immunohistochemical staining of RUNX2, COL-1 and CD31 (Figure 7b). The findings demonstrated a significant increase in immunofluorescence (RUNX2 and COL-1) in the CSMP-ZnO (5) group, with a well-organized distribution around the osteoblasts. This suggests that the controlled release of zinc may enhance the expression of RUNX2 and COL-1, thereby stimulating specific biological processes. Furthermore, the positive staining of CD31 was significantly improved in the CSMP-ZnO (5) hydrogel group compared to other groups. Therefore, the CSMP-ZnO (5) hydrogel could significantly promote bone and vascular regeneration.

## 4 Discussion

In this study, we followed Chen et al.'s method to prepare CSMP [15]. First, methacrylic anhydride reacted with CS to obtain CSMA. The

CSMA solution was directly added to the PS mix solution in the second phosphate step. Subsequently, we added ZnO-NPs to the CSMP solution, and the phosphate groups on CSMP bound with  $Zn^{2+}$  through chelation. In this hydrogel, the PS was grafted onto CS to provide phosphate groups to chelate with ZnO-NPs. SEM images showed that the porous structure of CSMP hydrogel, with pore sizes ranging from 50 to 100  $\mu m$ , is more suitable for cell and tissue growth and nutrient and metabolite transport, waste removal, and oxygen diffusion (52). For bone graft materials, mechanical properties, like compressive strength, play a crucial role in bone regeneration (53). In addition, with an increase in ZnO-NPs, the maximum compressive strength of CSMP-ZnO rose, possibly due to ZnO-NPs acting as cross-linkers in this hydrogel system. Thus, with more ZnO-NPs in the hydrogel, the cross-linking sites and degree were increased, improving the compression property (54). Due to the weakly acidic nature of the CSMP solution, a small amount of ZnO was dissolved during the formation of the CSMP-ZnO hydrogel. However, when most of the phosphate groups were bound to ZnO, the dissolution of ZnO will stop. Throughout the experiment, it was found that the cross-linking degree of CSMP-ZnO (5) hydrogel was higher, resulting in better mechanical properties. However, the compressive strength of CSMP-ZnO (10) was reduced, possibly because some ZnO-NPs did not combine with the hydrogel. When ZnO NPs were added at a concentration of 10 mg/mL, the maximum compressive strength and modulus decreased. This may be because ZnO-NPs are not hard-phase structures.

For bone repair materials, excellent biocompatibility means that the implants can promote the development of tissues and cells in the

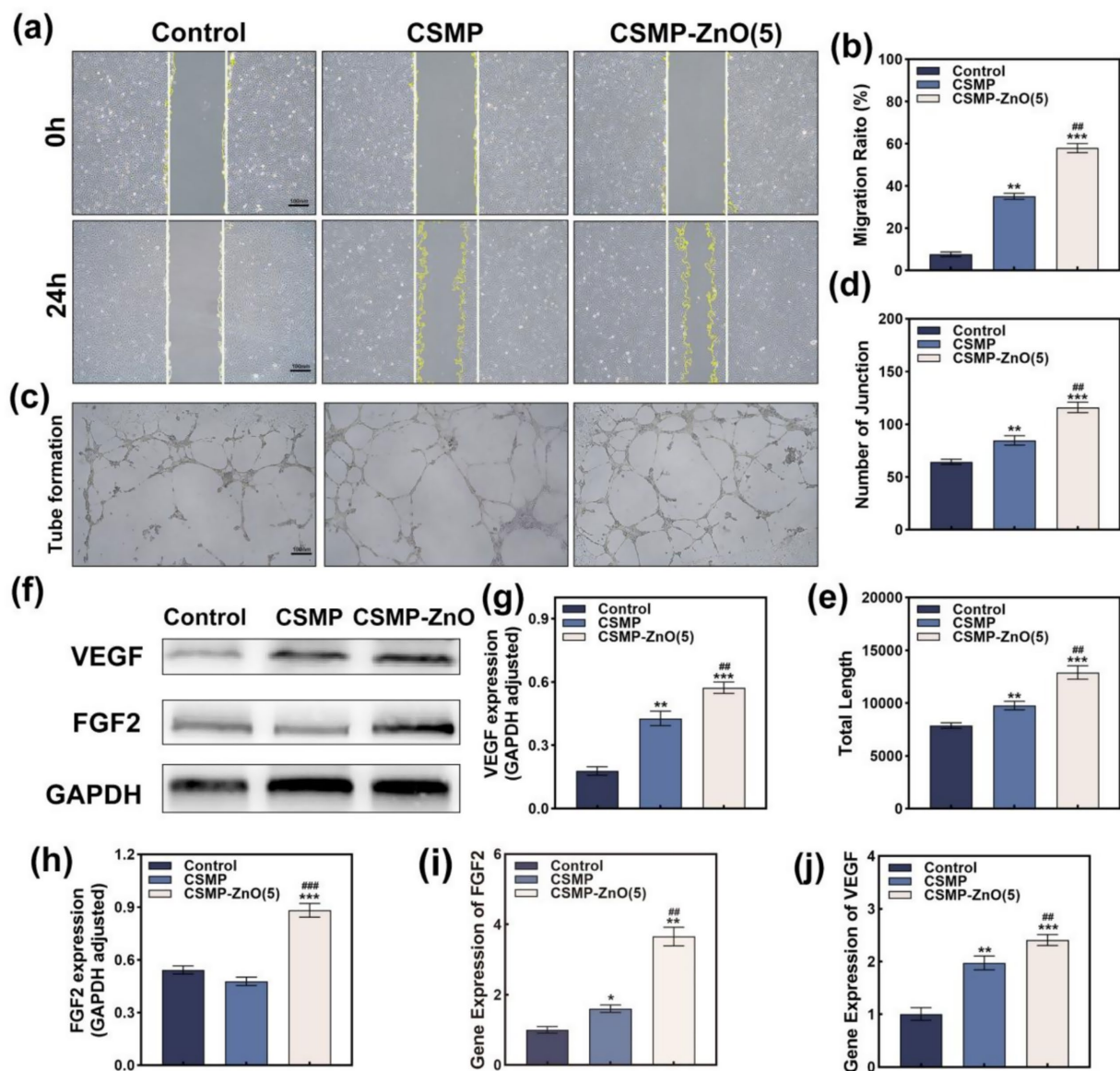


FIGURE 5

(a) Scratch assay and (b) corresponding quantitative analysis evaluating the migration activity of HUVECs. (c) Optical microscope images of Matrigel experiment evaluating the tube formation ability of HUVECs. (d,e) Quantitative analysis of the number of joint and total length. (f–h) Angiogenic protein (VEGF and FGF2) expression of HUVECs evaluated by WB. (i,j) Angiogenic gene (VEGF, FGF2) expression of HUVECs evaluated by PCR. Data are presented as mean values  $\pm$  SD ( $n = 3$ ). \*Compared with control. #Compared with CSMP. \* $p < 0.05$ , \*\* $p < 0.01$ , \*\*\* $p < 0.001$ ; # $p < 0.05$ , ## $p < 0.01$ , ### $p < 0.001$ .

bone defects environment, such as the proliferation of osteogenic-related cells and the differentiation of osteocytes. The application of ZnO-NPs *in vivo* is also considered safe. Our results indicate that CSMP and CSMP-ZnO hydrogels did not inhibit cell proliferation and have good cell adhesion properties. The rate of bone regeneration is significantly influenced by the impact of implants on cellular osteogenic differentiation, and the nature of bone as a mineralized connective tissue depends on the function and interaction of the cells with the extracellular matrix. The functional role of osteoblasts in bone formation is divided into three main stages. The first stage is the adhesion and proliferation of osteoblasts, and previous experiments have demonstrated that CSMP-ZnO hydrogel can promote the proliferation and adhesion of rBMSCs osteogenic precursor cells. The

second stage is osteogenic differentiation, which is the process of differentiation and maturation of osteoblasts from osteogenic precursor cells. In the third stage, the extracellular matrix mineralization, fully developed osteoblasts create a bone matrix by depositing calcium and phosphorus (55, 56). In this study, the CSMP-ZnO hydrogel promoted the expression of *COL1*, *RUNX2*, *BMP2*, *Smad1*, and *ALP* and the expression of *COL1*, *RUNX2*, and *BMP2* proteins in rBMSCs. Zinc can influence bone formation in the human body through various pathways. The results have indicated that zinc can enhance bone formation by regulating osteoblast-specific transcription factor 2 expression, increasing osteocalcin synthesis, type I collagen, and alkaline phosphatase activity, as well as increasing the accumulation of calcium and phosphorus. Zn<sup>2+</sup>

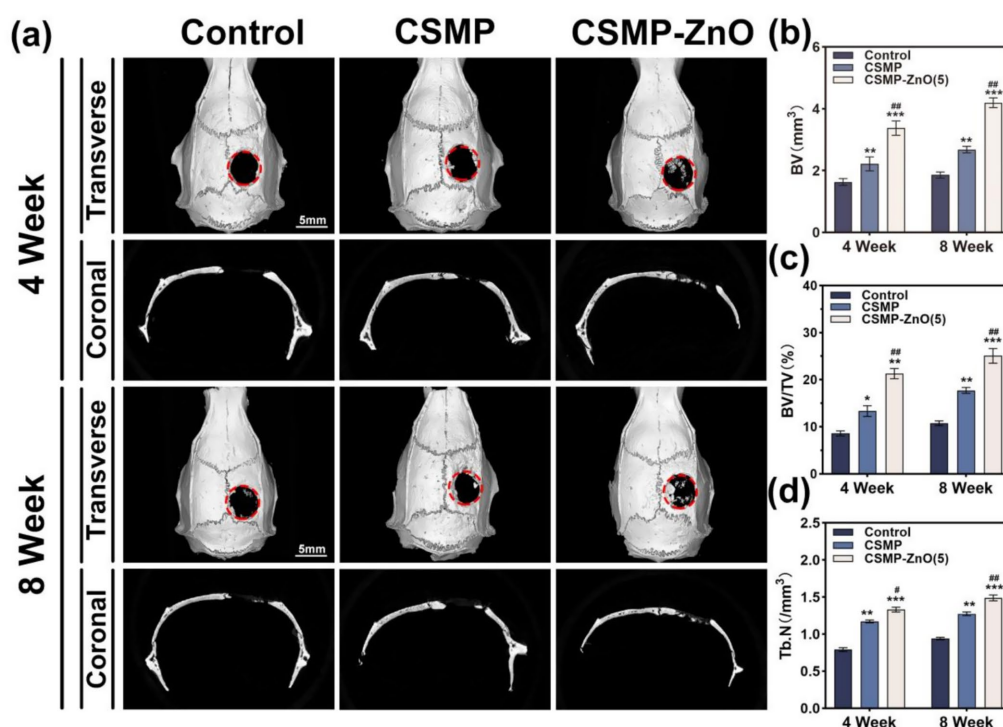


FIGURE 6

Micro-CT of new regenerated bone for the hydrogels implanted in the SD rat 5 mm critical-sized cranial defect for 4 and 8 weeks. (a) Micro-CT images. (b–d) New bone volume (BV), New bone volume/tissue volume (BV/TV) ratios and Trabecular bone number (Tb.N) in the critical-sized area calculated from micro-CT assessment. \*Compared with control. #Compared with CSMP. Data are presented as mean values  $\pm$  SD ( $n = 3$ ). \* $p < 0.05$ , \*\* $p < 0.01$ , \*\*\* $p < 0.001$ ; # $p < 0.05$ , ## $p < 0.01$ , ### $p < 0.001$ .

effectively enhances the absorption and utilization of crucial minerals like calcium and phosphorus while activating matrix metalloproteinases. This promotes bone metabolic balance and strength, ultimately leading to an increase in bone density. These factors collectively play a pivotal role in osteogenesis and significantly contribute to new bone growth (57–59). ALP is a typical protein product produced during osteoblast proliferation, differentiation, and extracellular matrix maturation; therefore, ALP activity is often an indicator of early osteoblast differentiation (60). ALP staining showed that CSMP-ZnO hydrogel could significantly fasten cell differentiation and maturation. The calcium nodule staining results indicated a significant advancement when extracellular matrix mineralization occurred in the CSMP-ZnO hydrogel. To evaluate the bone repair capability and bioactivity of CSMP-ZnO hydrogel *in vivo*, we implanted it into the skull of rats. We analyzed the differences in bone growth between CSMP and CSMP-ZnO at various time points post-implantation. Micro-CT analysis indicates that the CSMP-ZnO hydrogel group exhibited greater new bone volume and a higher number of trabeculae than the other two groups. Observations from H&E and Masson's staining revealed that CSMP-ZnO hydrogel can promote the formation of collagen, blood vessels, and bone matrix at the bone defect site. *COL1* and *ALP* immunohistochemical staining also confirmed this result. Compared to CSMP hydrogel and control groups, the CSMP-ZnO hydrogel group showed a significant increase in positive staining for new bone and osteoblasts, suggesting that CSMP-ZnO hydrogel can markedly promote bone regeneration and bone defect repair, and exhibit positive effects on osteogenesis and new bone formation.

Timely and adequate angiogenesis during bone defect repair is also crucial to the speed of bone repair. Neovascularization not only provides a large amount of oxygen and nutrients, but also a constant supply of bone progenitor cells and bone units. In this study, the effects of ZnO on HUVECs were analyzed via scratch assay, transwell assay and tube formation assay, and the results showed that the ZnO enhanced the migration ability and tube formation of HUVECs compared with CSMP group. Moreover, the transcription levels of *VEGF* and *FGF2* were most significantly upregulated in CSMP-ZnO group, which is attributed to the release of  $Zn^{2+}$  from nano ZnO-NPs. Similar results were also obtained in WB by detecting the expression of the angiogenic-related protein.

In conclusion, the *in vivo* and *in vitro* experimental results demonstrate that the ZnO-NPs-doped phosphorylated CSMP hydrogel exhibits good bioactivity, osteogenic properties, and angiogenic properties.

## 5 Study limitations

However, the present study has limitations. First, the exploration of the osteogenic mechanism of CSMP-ZnO hydrogels in this experiment is preliminary, relying solely on simple validation from other studies. To overcome this limitation, we suggest that future studies employ genomics or proteomics methods to comprehensively investigate the osteogenic mechanisms, which will provide a deeper understanding of the

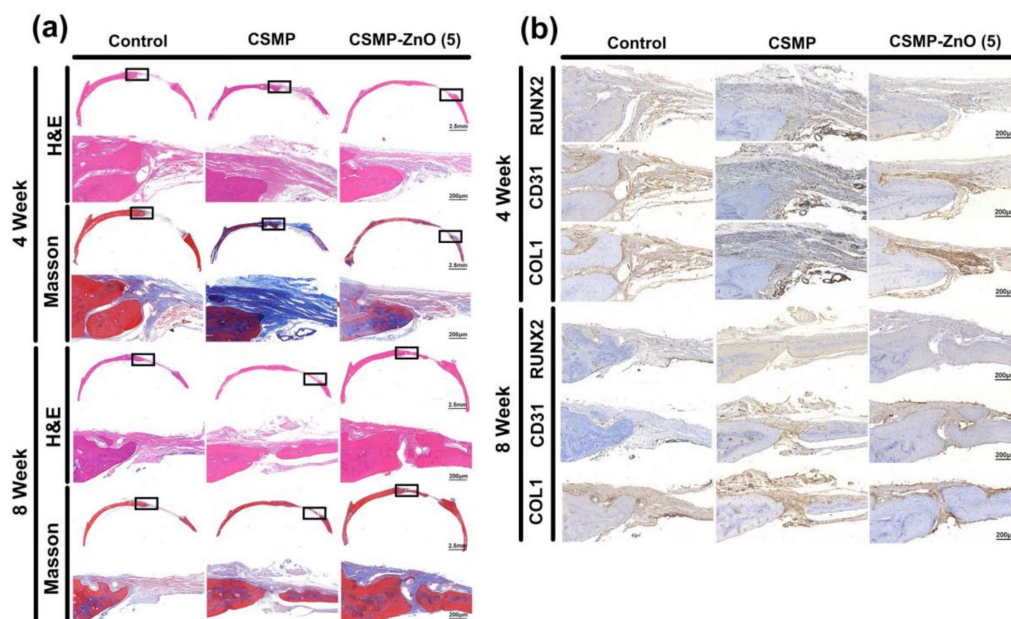


FIGURE 7

Section staining for the critical-sized cranial defect area after hydrogels implanted for 4 and 8 weeks. (a) Representative hematoxylin and eosin (H&E) and Masson trichrome stained images for the defect area after hydrogels implanted for 4 and 8 weeks. (b) Immunohistochemical staining of the osteogenic marker RUNX2, COL-1 and CD31.

underlying biological processes. Additionally, we acknowledge that the impact of immune regulation on bone formation was not investigated in our current experiment. Given the positive role of immune regulation in bone formation, we propose that future experiments should explore the influence of CSMP-ZnO on immune regulation during bone regeneration. This will not only enhance our understanding of the material's biological effects but also potentially uncover new therapeutic targets.

## 6 Conclusion

Thus, we designed novel CSMP-ZnO hydrogel scaffolds and used them for local bone regeneration for the first time. The porous structure of CSMP-ZnO scaffolds enhanced cell adhesion and showed good binding with bone tissue to promote bone regeneration. The incorporation of ZnO nanoparticles improved the bulk modulus, compression stress, anti-swelling properties. Moreover, the CSMP-ZnO scaffold possesses the sustained release of zinc ions, and the release of zinc ions further promote the osteogenesis and angiogenesis performance. The CSMP-ZnO hydrogel scaffolds significantly promoted osteogenic activity through the BMP2-Smad1 signaling pathway, and increased the expression levels of osteogenic proteins (COL-1, BMP2, RUNX2) and genes (*COL-1*, *BMP2*, *RUNX2*, *Smad1*, *ALP*). In addition, *in vivo* experiments showed that the CSMP-ZnO hydrogel significantly promoted bone regeneration. The CSMP-ZnO hydrogel superior to the CSMP hydrogel in enhancing the growth, formation of bone tissue by rBMSCs, and the regeneration of bone. This study demonstrated that incorporating ZnO into hydrogels demonstrates a promising strategy for bone regeneration, thus serving as a new strategy for bone tissue engineering and regeneration in the future.

## Data availability statement

The original contributions presented in the study are included in the article/[Supplementary material](#), further inquiries can be directed to the corresponding authors.

## Ethics statement

Ethical approval was not required for the studies on humans in accordance with the local legislation and institutional requirements because only commercially available established cell lines were used. The animal study was approved by Institutional Animal Ethics Committee of Ningbo University Laboratory Animal Center. The study was conducted in accordance with the local legislation and institutional requirements.

## Author contributions

LeL: Writing – original draft. DX: Methodology, Writing – original draft. CH: Supervision, Writing – original draft. ZL: Data curation, Writing – original draft. HY: Software, Writing – original draft. BL: Validation, Writing – original draft. KZ: Conceptualization, Writing – original draft. LiL: Funding acquisition, Writing – review & editing. KG: Writing – review & editing.

## Funding

The author(s) declare that financial support was received for the research and/or publication of this article. This study was supported

by the Ningbo Top Medical and Health Research Program (Grant Number: 2022020102)

## Conflict of interest

The authors declare that the research was conducted in the absence of any commercial or financial relationships that could be construed as a potential conflict of interest.

The handling editor WM declared a past co-authorship with the author DX.

## Generative AI statement

The authors declare that no Gen AI was used in the creation of this manuscript.

Any alternative text (alt text) provided alongside figures in this article has been generated by Frontiers with the support of artificial

## References

- El-Rashidy, AA, Roether, JA, Harhaus, L, Kneser, U, and Boccaccini, AR. Regenerating bone with bioactive glass scaffolds: a review of in vivo studies in bone defect models. *Acta Biomater.* (2017) 62:1–28. doi: 10.1016/j.actbio.2017.08.030
- Liu, Z, Yuan, X, Fernandes, G, Dziak, R, Ionita, CN, Li, C, et al. The combination of nano-calcium sulfate/platelet rich plasma gel scaffold with BMP2 gene-modified mesenchymal stem cells promotes bone regeneration in rat critical-sized calvarial defects. *Stem Cell Res Ther.* (2017) 8:122. doi: 10.1186/s13287-017-0574-6
- Li, X, Zhang, R, Tan, X, Li, B, Liu, Y, and Wang, X. Synthesis and evaluation of BMMSC-seeded BMP-6/nHAG/GMS scaffolds for bone regeneration. *Int J Med Sci.* (2019) 16:1007–17. doi: 10.7150/ijms.31966
- Dimitriou, R, Jones, E, McGonagle, D, and Giannoudis, PV. Bone regeneration: current concepts and future directions. *BMC Med.* (2011) 9:66. doi: 10.1186/1741-7015-9-66
- Scheller, EL, Krebsbach, PH, and Kohn, DH. Tissue engineering: state of the art in oral rehabilitation. *J Oral Rehabil.* (2009) 36:368–89. doi: 10.1111/j.1365-2842.2009.01939.x
- Amiryaghoubi, N, Fathi, M, Pesyan, NN, Samiei, M, Barar, J, and Omid, Y. Bioactive polymeric scaffolds for osteogenic repair and bone regenerative medicine. *Med Res Rev.* (2020) 40:1833–70. doi: 10.1002/med.21672
- Eslaminejad, MB. Mesenchymal stem cells as a potent cell source for articular cartilage regeneration. *WJSC.* (2014) 6:344. doi: 10.4252/wjsc.v6.i3.344
- Rao, SH, Harini, B, Shadamarshan, RPK, Balagangadharan, K, and Selvamurugan, N. Natural and synthetic polymers/bioceramics/bioactive compounds-mediated cell signalling in bone tissue engineering. *Int J Biol Macromol.* (2018) 110:88–96. doi: 10.1016/j.ijbiomac.2017.09.029
- Dec, P, Modrzewski, A, and Pawlik, A. Existing and novel biomaterials for bone tissue engineering. *Int J Mol Sci.* (2022) 24:529. doi: 10.3390/ijms24010529
- Sivakumar, PM, Yetisgin, AA, Demir, E, Sahin, SB, and Cetinel, S. Polysaccharide-bioceramic composites for bone tissue engineering: a review. *Int J Biol Macromol.* (2023) 250:126237. doi: 10.1016/j.ijbiomac.2023.126237
- Wang, Y, Wang, J, Gao, R, Liu, X, Feng, Z, Zhang, C, et al. Biomimetic glycopeptide hydrogel coated PCL/nHA scaffold for enhanced cranial bone regeneration via macrophage M2 polarization-induced osteo-immunomodulation. *Biomaterials.* (2022) 285:121538. doi: 10.1016/j.biomaterials.2022.121538
- Hwangbo, H, Lee, J, and Kim, G. Mechanically and biologically enhanced 3D-printed HA/PLLA/dECM biocomposites for bone tissue engineering. *Int J Biol Macromol.* (2022) 218:9–21. doi: 10.1016/j.ijbiomac.2022.07.040
- Zhou, B, Jiang, X, Zhou, X, Tan, W, Luo, H, Lei, S, et al. GelMA-based bioactive hydrogel scaffolds with multiple bone defect repair functions: therapeutic strategies and recent advances. *Biomater Res.* (2023) 27:86. doi: 10.1186/s40824-023-00422-6
- Sivakumar, PM, Yetisgin, AA, Sahin, SB, Demir, E, and Cetinel, S. Bone tissue engineering: anionic polysaccharides as promising scaffolds. *Carbohydr Polym.* (2022) 283:119142. doi: 10.1016/j.carbpol.2022.119142
- Chen, Y, Sheng, W, Lin, J, Fang, C, Deng, J, Zhang, P, et al. Magnesium oxide nanoparticle coordinated phosphate-functionalized chitosan injectable hydrogel for osteogenesis and angiogenesis in bone regeneration. *ACS Appl Mater Interfaces.* (2022) 14:7592–608. doi: 10.1021/acscami.1c21260

intelligence and reasonable efforts have been made to ensure accuracy, including review by the authors wherever possible. If you identify any issues, please contact us.

## Publisher's note

All claims expressed in this article are solely those of the authors and do not necessarily represent those of their affiliated organizations, or those of the publisher, the editors and the reviewers. Any product that may be evaluated in this article, or claim that may be made by its manufacturer, is not guaranteed or endorsed by the publisher.

## Supplementary material

The Supplementary material for this article can be found online at: <https://www.frontiersin.org/articles/10.3389/fmed.2025.1729401/full#supplementary-material>

- Ge, Y-W, Fan, Z-H, Ke, Q-F, Guo, Y-P, Zhang, C-Q, and Jia, W-T. SrFe<sub>2</sub>O<sub>9</sub>-doped nano-layered double hydroxide/chitosan layered scaffolds with a nacre-mimetic architecture guide in situ bone ingrowth and regulate bone homeostasis. *Materials Today Bio.* (2022) 16:100362. doi: 10.1016/j.mtbio.2022.100362
- Kang, Y, Xu, J, Meng, L, Su, Y, Fang, H, Liu, J, et al. 3D bioprinting of dECM/gel/QCS/nHAp hybrid scaffolds laden with mesenchymal stem cell-derived exosomes to improve angiogenesis and osteogenesis. *Biofabrication.* (2023) 15:024103. doi: 10.1088/1758-5090/acb6b8
- Aguilar, A, Zein, N, Harmouch, E, Hafdi, B, Bornert, F, Offner, D, et al. Application of chitosan in bone and dental engineering. *Molecules.* (2019) 24:3009. doi: 10.3390/molecules24163009
- Gholap, AD, Rojekar, S, Kapare, HS, Vishwakarma, N, Raikwar, S, Garkal, A, et al. Chitosan scaffolds: expanding horizons in biomedical applications. *Carbohydr Polym.* (2024) 323:121394. doi: 10.1016/j.carbpol.2023.121394
- Brun, P, Zamuner, A, Battocchio, C, Cassari, L, Todesco, M, Graziani, V, et al. Bio-functionalized chitosan for bone tissue engineering. *IJMS.* (2021) 22:5916. doi: 10.3390/ijms22115916
- Zhu, Y, Zhang, Y, and Zhou, Y. Application progress of modified chitosan and its composite biomaterials for bone tissue engineering. *IJMS.* (2022) 23:6574. doi: 10.3390/ijms23126574
- LogithKumar, R, KeshavNarayan, A, Dhivya, S, Chawla, A, Saravanan, S, and Selvamurugan, N. A review of chitosan and its derivatives in bone tissue engineering. *Carbohydr Polym.* (2016) 151:172–88. doi: 10.1016/j.carbpol.2016.05.049
- Rezaei, FS, Sharifianjazi, F, Esmaeilkhanian, A, and Salehi, E. Chitosan films and scaffolds for regenerative medicine applications: a review. *Carbohydr Polym.* (2021) 273:118631. doi: 10.1016/j.carbpol.2021.118631
- Rahimi, M, Mir, SM, Baghban, R, Charmi, G, Plummer, CM, Shafiei-Irannejad, V, et al. Chitosan-based biomaterials for the treatment of bone disorders. *Int J Biol Macromol.* (2022) 215:346–67. doi: 10.1016/j.ijbiomac.2022.06.079
- Sheng, W, Qin, H, Wang, T, Zhao, J, Fang, C, Zhang, P, et al. Advanced phosphocreatine-grafted chitosan hydrogel promote wound healing by macrophage modulation. *Front Bioeng Biotechnol.* (2023) 11:1199939. doi: 10.3389/fbioe.2023.1199939
- Céspedes-Valenzuela, DN, Sánchez-Rentería, S, Cifuentes, J, Gantiva-Díaz, M, Serna, JA, Reyes, LH, et al. Preparation and characterization of an injectable and photo-responsive chitosan methacrylate/graphene oxide hydrogel: potential applications in bone tissue adhesion and repair. *Polymers.* (2021) 14:126. doi: 10.3390/polym14010126
- Rył, A, Miazgowski, T, Szylińska, A, Turon-Skrzypińska, A, Jurewicz, A, Bohatyrewicz, A, et al. Bone health in aging men: does zinc and cuprum level matter? *Biomolecules.* (2021) 11:237. doi: 10.3390/biom11020237
- Molenda, M, and Kolmas, J. The role of zinc in bone tissue health and regeneration—a review. *Biol Trace Elem Res.* (2023) 201:5640–51. doi: 10.1007/s12011-023-03631-1
- Kambe, T, Tsuji, T, Hashimoto, A, and Itsumura, N. The physiological, biochemical, and molecular roles of zinc transporters in zinc homeostasis and metabolism. *Physiol Rev.* (2015) 95:749–84. doi: 10.1152/physrev.00035.2014

30. Ji, Z, Wan, Y, Zou, Y, Wang, H, Liang, X, and Liu, P. Dual-release 3D-printed porous Ti-6Al-4V implant with drug-eluting photothermal micro-nanotopographies: combating osteosarcoma recurrence, infections, and enhancing osteogenesis. *Biomaterials*. (2026) 327:123749. doi: 10.1016/j.biomaterials.2025.123749
31. Chen, L, Zhou, C, Xie, Q, Xia, L, Liu, L, Bao, W, et al. Zinc doped synthetic polymer composites for bone regeneration: a promising strategy to repair bone defects. *IJN*. (2025) 20:8567–86. doi: 10.2147/IJN.S512994
32. O'Connor, JP, Kanjilal, D, Teitelbaum, M, Lin, SS, and Cottrell, JA. Zinc as a therapeutic agent in bone regeneration. *Materials*. (2020) 13:2211. doi: 10.3390/ma13102211
33. Rehder, F, Arango-Ospina, M, Decker, S, Saur, M, Kunisch, E, Moghaddam, A, et al. The addition of zinc to the ICIE16-bioactive glass composition enhances osteogenic differentiation and matrix formation of human bone marrow-derived mesenchymal stromal cells. *Biomimetics*. (2024) 9:53. doi: 10.3390/biomimetics9010053
34. Meng, G, Wu, X, Yao, R, He, J, Yao, W, and Wu, F. Effect of zinc substitution in hydroxyapatite coating on osteoblast and osteoclast differentiation under osteoblast/osteoclast co-culture. *Regenerat Biomater*. (2019) 6:349–59. doi: 10.1093/rb/rbz001
35. Wang, S, Gu, R, Wang, F, Zhao, X, Yang, F, Xu, Y, et al. 3D-printed PCL/zinc scaffolds for bone regeneration with a dose-dependent effect on osteogenesis and osteoclastogenesis. *Materials Today Bio*. (2022) 13:100202. doi: 10.1016/j.mtbio.2021.100202
36. Cho, Y-E, and Kwun, I-S. Zinc upregulates bone-specific transcription factor Runx2 expression via BMP-2 signaling and smad-1 phosphorylation in osteoblasts. *J Nutr Health*. (2018) 51:23. doi: 10.4163/jnh.2018.51.1.23
37. Zarei, A, and Farazin, A. Synergizing additive manufacturing and machine learning for advanced hydroxyapatite scaffold design in bone regeneration. *J Aust Ceram Soc*. (2025) 61:797–813. doi: 10.1007/s41779-024-01084-w
38. P V S, Mathew, AM, Vignesh, K, Swathi, CM, Kadalmani, B, and Pattanayak, DK. Unveiling the role of zinc on the nanotitanium network in determining the *in vitro* and *in vivo* characteristics of titanium-based orthopedic implants. *ACS Appl Mater Interfaces* (2025) 17:56773–56785. doi: 10.1021/acsmi.5c13421
39. Laurenti, M, and Cauda, V. ZnO nanostructures for tissue engineering applications. *Nano*. (2017) 7:374. doi: 10.3390/nano7110374
40. Shitole, AA, Raut, PW, Sharma, N, Giram, P, Khandwekar, AP, and Garnaik, B. Electrospun polycaprolactone/hydroxyapatite/ZnO nanofibers as potential biomaterials for bone tissue regeneration. *J Mater Sci Mater Med*. (2019) 30:51. doi: 10.1007/s10856-019-6255-5
41. Qiu, D, Zhou, P, Kang, J, Chen, Z, Xu, Z, Yang, H, et al. ZnO nanoparticle modified chitosan/borosilicate bioglass composite scaffold for inhibiting bacterial infection and promoting bone regeneration. *Biomed Mater*. (2022) 17:065023. doi: 10.1088/1748-605X/ac99c5
42. Zhang, Y, Li, Z, Guo, B, Wang, Q, Chen, L, Zhu, L, et al. A zinc oxide nanowire-modified mineralized collagen scaffold promotes infectious bone regeneration. *Small*. (2024) 20:e2309230. doi: 10.1002/smll.202309230
43. He, G, Nie, J-J, Liu, X, Ding, Z, Luo, P, Liu, Y, et al. Zinc oxide nanoparticles inhibit osteosarcoma metastasis by downregulating  $\beta$ -catenin via HIF-1 $\alpha$ /BNIP3/LC3B-mediated mitophagy pathway. *Bioact Mater*. (2023) 19:690–702. doi: 10.1016/j.bioactmat.2022.05.006
44. Sun, Y, Yao, X, Zhang, Y, Zhang, W, Zhu, C, Shen, C, et al. Zinc oxide-copper sulfide nanozyme hydrogels for bone defect repair by modulating the bone immune microenvironment and promoting osteogenesis/angiogenesis. *ACS Appl Mater Interfaces*. (2025) 17:29100–18. doi: 10.1021/acsmi.4c23069
45. Streich, S, Higuchi, J, Opalińska, A, Wojnarowicz, J, Giovanoli, P, Łojkowski, W, et al. Ultrasonic coating of poly(D,L-lactic acid)/poly(lactic-co-glycolic acid) electrospun fibers with ZnO nanoparticles to increase angiogenesis in the CAM assay. *Biomedicine*. (2024) 12:1155. doi: 10.3390/biomedicine12061155
46. Li, T, Peng, M, Yang, Z, Zhou, X, Deng, Y, Jiang, C, et al. 3D-printed IFN- $\gamma$ -loading calcium silicate- $\beta$ -tricalcium phosphate scaffold sequentially activates M1 and M2 polarization of macrophages to promote vascularization of tissue engineering bone. *Acta Biomater*. (2018) 71:96–107. doi: 10.1016/j.actbio.2018.03.012
47. Zhan, Y, Fu, W, Xing, Y, Ma, X, and Chen, C. Advances in versatile anti-swelling polymer hydrogels. *Mater Sci Eng C*. (2021) 127:112208. doi: 10.1016/j.msec.2021.112208
48. Wang, L, Wang, C, Wu, S, Fan, Y, and Li, X. Influence of the mechanical properties of biomaterials on degradability, cell behaviors and signaling pathways: current progress and challenges. *Biomater Sci*. (2020) 8:2714–33. doi: 10.1039/D0BM00269K
49. Ai, Y, She, W, Wu, S, Shao, Q, Jiang, Z, Chen, P, et al. AM1241-loaded poly(ethylene glycol)-dithiothreitol hydrogel repairs cranial bone defects by promoting vascular endothelial growth factor and COL-1 expression. *Front Cell Dev Biol*. (2022) 10:888598. doi: 10.3389/fcell.2022.888598
50. Komori, T. Whole aspect of Runx2 functions in skeletal development. *IJMS*. (2022) 23:5776. doi: 10.3390/ijms23105776
51. Choi, H, Jeong, B-C, Kook, M-S, and Koh, J-T. Betulinic acid synergically enhances BMP2-induced bone formation via stimulating smad 1/5/8 and p38 pathways. *J Biomed Sci*. (2016) 23:45. doi: 10.1186/s12929-016-0260-5
52. Wei, X, Zhou, W, Tang, Z, Wu, H, Liu, Y, Dong, H, et al. Magnesium surface-activated 3D printed porous PEEK scaffolds for *in vivo* osseointegration by promoting angiogenesis and osteogenesis. *Bioact Mater*. (2023) 20:16–28. doi: 10.1016/j.bioactmat.2022.05.011
53. Shi, C, Hou, X, Zhao, D, Wang, H, Guo, R, and Zhou, Y. Preparation of the bioglass/chitosan-alginate composite scaffolds with high bioactivity and mechanical properties as bone graft materials. *J Mech Behav Biomed Mater*. (2022) 126:105062. doi: 10.1016/j.jmbbm.2021.105062
54. Chen, R, Chen, H-B, Xue, P-P, Yang, W-G, Luo, L-Z, Tong, M-Q, et al. HA/MgO nanocrystal-based hybrid hydrogel with high mechanical strength and osteoinductive potential for bone reconstruction in diabetic rats. *J Mater Chem B*. (2021) 9:1107–22. doi: 10.1039/D0TB02553D
55. Tresguerres, FGE, Torres, J, López-Quiles, J, Hernández, G, Vega, JA, and Tresguerres, IF. The osteocyte: a multifunctional cell within the bone. *Ann Anat Anatomisc Anzeiger*. (2020) 227:151422. doi: 10.1016/j.aanat.2019.151422
56. Fonseca, H, Moreira-Gonçalves, D, Coriolano, H-JA, and Duarte, JA. Bone quality: the determinants of bone strength and fragility. *Sports Med*. (2014) 44:37–53. doi: 10.1007/s40279-013-0100-7
57. Zhang, Z, Jia, B, Yang, H, Han, Y, Wu, Q, Dai, K, et al. Biodegradable ZnLiCa ternary alloys for critical-sized bone defect regeneration at load-bearing sites: *in vitro* and *in vivo* studies. *Bioact Mater*. (2021) 6:3999–4013. doi: 10.1016/j.bioactmat.2021.03.045
58. Fu, X, Li, Y, Huang, T, Yu, Z, Ma, K, Yang, M, et al. Runx2/osterix and zinc uptake synergize to orchestrate osteogenic differentiation and citrate containing bone apatite formation. *Adv Sci*. (2018) 5:1700755. doi: 10.1002/advs.201700755
59. Summonte, S, Sanchez Armengol, E, Ricci, F, Sandmeier, M, Hock, N, Güclü-Tuncyüz, A, et al. Phosphatase-degradable nanoparticles providing sustained drug release. *Int J Pharm*. (2024) 654:123983. doi: 10.1016/j.ijpharm.2024.123983
60. Li, W, Zhang, S, Liu, J, Liu, Y, and Liang, Q. Vitamin K2 stimulates Mc3T3-E1 osteoblast differentiation and mineralization through autophagy induction. *Mol Med Rep*. (2019) 19:3676–84. doi: 10.3892/mmr.2019.10040